NANO LETTERS

2001
Vol. 1, No. 10
541−549

Ferrocene-Based Nanoelectronics: 2,5-Diethynylpyridine as a Reversible Switching Element

Chaiwat Engtrakul and Lawrence R. Sita*

Department of Chemistry and Biochemistry, University of Maryland, College Park, Maryland 20742

Received May 30, 2001; *Revised Manuscript Received July 30, 2001*

ABSTRACT

A new strategy is presented for the construction of a ferrocene-based molecular diode that operates by an electron-hopping mechanism. Key to this design is implementation of the asymmetric 2,5-diethynylpyridine bridging unit that serves to reversibly switch the system between two states. Results of investigations of the molecular and electronic structures of the diferrocene complexes 1 and 2, which respectively serve as models for state 1 and state 2, establish that the criteria for the new strategy can likely be met with the 2,5-diethynylpyridine bridge.

Introduction. There is considerable optimism that molecules will eventually play key roles in the design and operation of future nanoscale electronic devices.[1] What these specific roles will be, however, is currently an open question that must be addressed by a variety of different approaches. Our strategy is to incorporate the known properties of ferrocene, Cp_2Fe ($Cp = \eta^5$-C_5H_5), a molecular system that has been extensively investigated for the past 50 years, into working prototypes of molecular diodes and transistors that can, in turn, be used for the construction of computational logic gates. The advantages of a ferrocene-based approach to molecular circuits are (1) ferrocene has a high degree of chemical and thermal stability in a variety of environments, (2) the ferrocene/ferrocenium redox couple is robust and can be reversibly cycled, (3) the redox potential of this couple is considerably lower than the oxidation or reduction potentials of pure organic molecules, and this feature should translate to lower turn-on voltages and much higher operating stabilities, (4) the redox potential can be easily tuned over a wide range by the judicious choice of substituents on the rings of the ferrocene moiety, and (5) a wealth of synthetic methods are available to construct a large variety of relatively complex ferrocene-based systems by concise routes that entail only a few synthetic steps.[2] A large body of work has also been performed in which the factors that control the rate of electron transfer within materials possessing multiple ferrocene sites have been investigated.[3] Indeed, on the basis of the extensive database of knowledge regarding ferrocene, we propose the molecular diode design shown in Scheme 1 in which "conduction" (i.e., electron transfer) is expected to proceed primarily through an electron-hopping mechanism involving distinct and spatially well-defined redox sites.[4] The advantage of a design that is based on electron-hopping conduction is that it should not be necessary to achieve the critical matching of electronic states for all elements in the conduction path, as is required for effective "through-bond" conduction involving electron tunneling by way of an electronic state that is delocalized over the entire length of the system.

The key design element of our ferrocene-based diode is the conjugated 2,5-diethynylpyridyl unit that links two ferrocenes together, as shown in Scheme 1. Given the length of this pyridyl spacer, the two ferrocenes should not be in direct electronic communication with one another,[3] and in this state (state 1), electron-hopping conduction should be able to proceed through the path connecting the two metal termini regardless of the potential bias. However, when a positive charge is fixed on the nitrogen atom of the pyridyl ring, state 2 is produced in which the two ferrocene groups now possess distinctly different redox potentials as a result of the charge being able to delocalize close to one ferrocene but not the other. This separation of formal potentials should now create a barrier for electron-hopping conduction when a forward bias is applied, as schematically shown to the right in Scheme 1. For the reverse bias, however, this barrier is absent and conduction can occur, thereby establishing a means not only for on/off switching of current (vis-à-vis, state 1 and state 2) but also for rectification of current while in state 2.

The design shown in Scheme 1 is unique in that, to the best of our knowledge, no one has yet established that an *asymmetric* bridging element, such as the 2,5-diethynylpyridine unit in our case, can perturb the electronic structure of two linked metal complexes evenly, thereby generating

10.1021/nl010038p CCC: $20.00
Published on Web 09/05/2001

Scheme 1

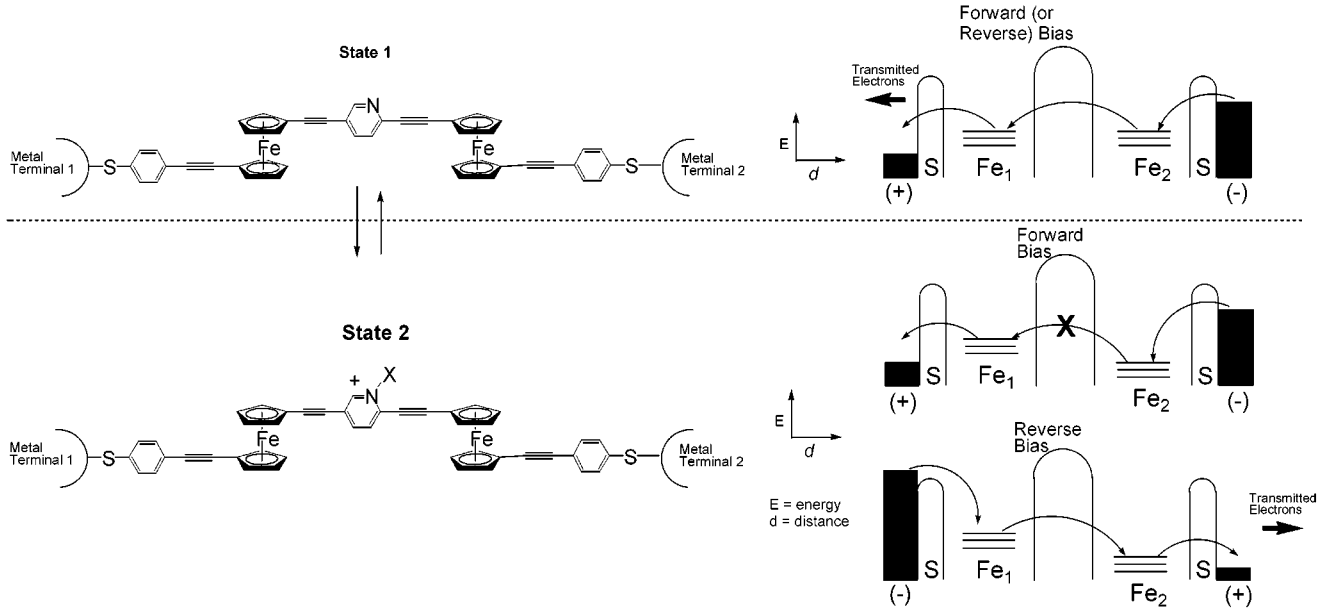

identical redox potentials for the two metal centers in what we distinguish as state 1. In turn, if an asymmetric bridging element can be so electronically isolated from the ferrocenes to allow for the condition of state 1, the question next becomes whether modification of this bridge can then have a dramatic enough effect on the redox potentials of the ferrocenes to establish state 2. To address these questions, we synthesized and characterized complexes **1** and **2** as

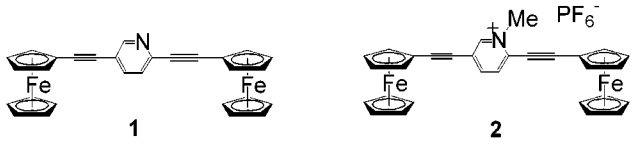

models for state 1 and state 2, respectively. Importantly, investigations of the molecular and electronic structures of these complexes by a variety of structural, optical, and electrochemical methods, as outlined below, have established that the criteria for the design of Scheme 1 can more than likely be met with the structures shown.

Results and Discussion. *Synthesis.* The syntheses of **1** and **2** were conducted in the straightforward manner shown in Scheme 2. Thus, palladium-catalyzed Sonogashira coupling of commercially available 2,5-dibromopyridine with 2 equiv of ethynylferrocene[5] yielded orange-red **1** in a 48% isolated yield. Methylation of the pyridyl nitrogen using methyl iodide, followed by anion exchange with tetrabutylammonium hexafluorophosphate then provided dark purple crystalline **2** in high yield (74%).

Although **1** and **2** can be readily obtained by these synthetic procedures, to probe the electronic structures of these model complexes in more detail, it was necessary to develop a regiospecific route to monoferrocene compounds bearing the 2,5-diethynylpyridine moiety in which the relative orientation of the pyridyl nitrogen atom with respect to the ferrocene group can be fixed with certainty. As shown by Scheme 3, this requirement was achieved by taking advantage of the differential coupling properties of 2,5-dibromopyridine vs 2-bromo-5-iodopyridine in the Sonogashira reaction. Thus, the palladium-catalyzed coupling of 1 equiv

Scheme 2[a]

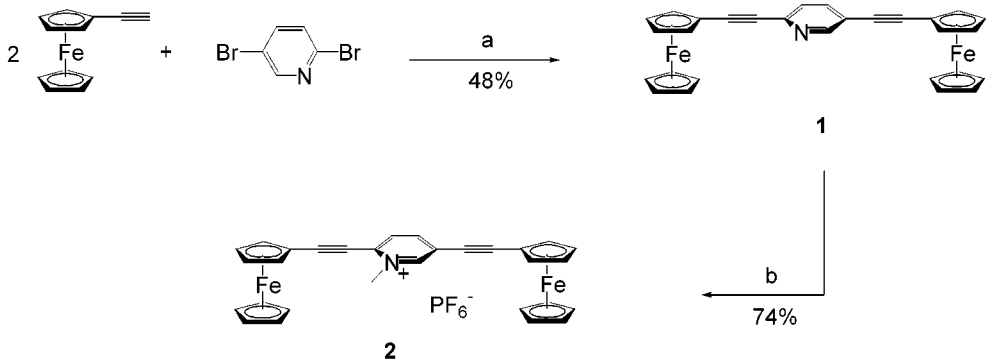

[a] Reagents: (a) $Pd(PPh_3)_2Cl_2$ (4 mol %), CuI (4 mol %), THF/Hunig's Base (1:1), 55 °C, 24 h. (b) (i) MeI, CH_2Cl_2/CH_3CN, 50 °C, 18 h. (ii) H_2O, NH_4PF_6.

Scheme 3[a]

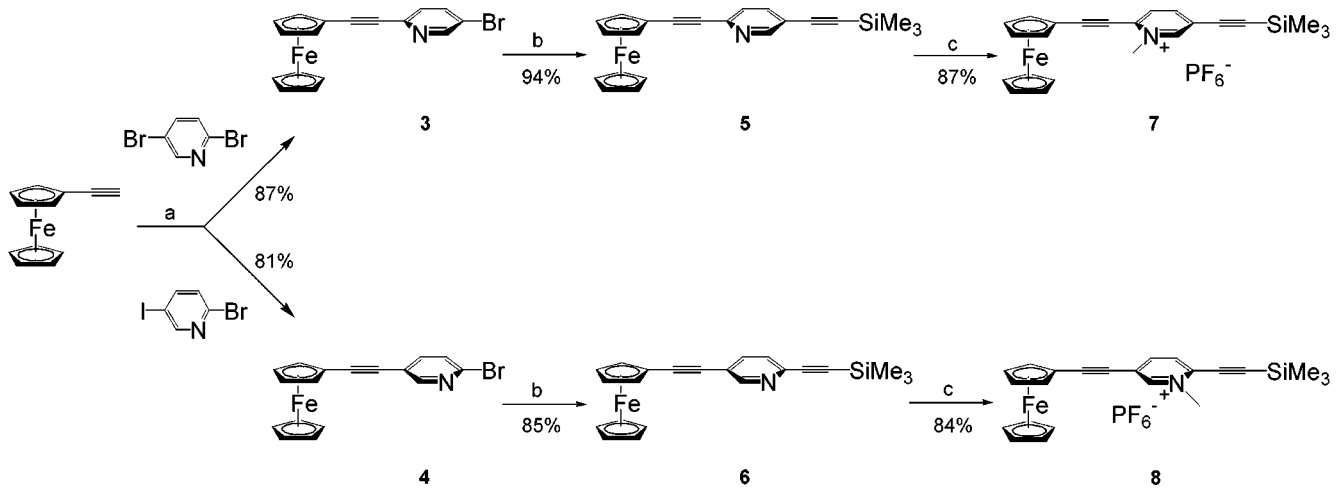

[a] Reagents: (a) $Pd(PPh_3)_2Cl_2$ (4 mol %), CuI (4 mol %), amine, 60 °C, 24 h. (b) Trimethylsilylacetylene, $Pd(PPh_3)_2Cl_2$ (4 mol %), CuI (4 mol %), THF/Hunig's Base (1:1), 60 °C, 48 h. (c) (i) MeI, CH_2Cl_2/CH_3CN, 50 °C, 18 h. (ii) H_2O, NH_4PF_6.

of ethynylferrocene with 2,5-dibromopyridine yielded the ethynylpyridine-derivatized ferrocene **3** as the sole product.[6] On the other hand, the same coupling reaction employing 2-bromo-5-iodopyridine [prepared through regioselective transhalogenation of 2,5-dibromopyridine, (i) 1 equiv of *n*-butyllithium, (ii) I_2, at −78 °C] provided the regioisomer **4**, once again in high yield and as the sole product. To establish with certainty the relative orientation of the pyridyl group in **3** and **4**, the crystal structure of the latter compound was determined by single-crystal X-ray crystallographic analysis. As Scheme 3 reveals, both **3** and **4** were then converted to their respective 2,5-diethynylpyridyl-derivatized monoferrocenes, **5** and **6**, through palladium-catalyzed coupling with trimethylsilylacetylene. Finally, compounds **5** and **6** were, in turn, methylated in high yield to provide the two isomeric pyridinium cations, **7** and **8**, that were isolated as their hexafluorophosphate salts.

Crystal Structures. Single-crystal X-ray crystallography was used to establish the relative ground-state perturbations of the pyridyl vs the pyridinium cation bridge on the molecular structures of the linked diferrocene systems of **1** and **2**. Figures 1 and 2 present the solid-state molecular structures for each of these compounds, while Table 1 provides a listing of selected bond lengths and angles for comparison purposes.[7] Interestingly, from these data, the feature that is perhaps of most interest is that very little difference is actually observed for the carbon−carbon bond lengths of **1** vs those of **2**. Indeed, apart from the difference seen in the relative orientation of the two ferrocene groups in going from **1** to **2**, which might arise from differences in crystal packing forces, the two compounds have nearly identical ground-state structures with respect to the conjugated bond path connecting the two ferrocene units. It is somewhat of interest, however, that for **1**, the central ring of the bridge is nearly coplanar with the cyclopentadienyl (Cp) rings of the ferrocenes (torsion angle: 2.7°), whereas for **2**, this ring is canted by 10° with respect to these moieties.

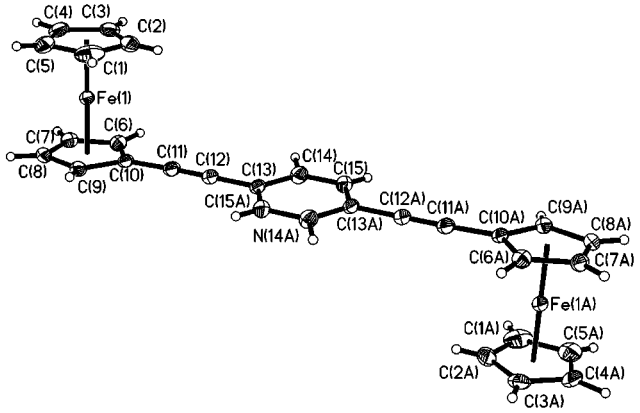

Figure 1. ORTEP representation (30% thermal ellipsoids) of the molecular structure of **1**. Hydrogen atoms are represented by spheres of arbitrary size. Atom numbers with the letter A suffix are related to the corresponding unlettered atoms via an inversion center. The pyridyl nitrogen atom has 50% occupancy at both positions C(14) and N(14A).

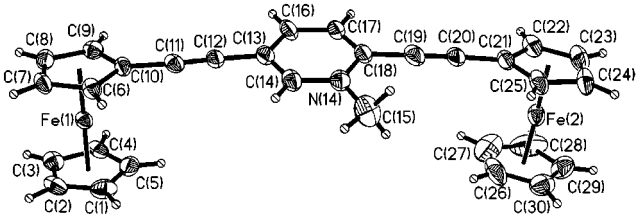

Figure 2. ORTEP representation (30% thermal ellipsoids) of the molecular structure of **2**. Hydrogen atoms are represented by spheres of arbitrary size. The PF_6 anion has been omitted for the sake of clarity.

Whether this difference is due to electronic factors or simply arises due to differences in crystal packing forces is difficult to ascertain on the basis of these structural data alone. To summarize then, the results of these structural studies are not sufficient to determine whether the strategy presented in Scheme 1 can be achieved with the 2,5-diethynylpyridyl group.

Table 1. Selected Bond Lengths (Å) and Torsion Angles (Deg) for Compounds **1** and **2**

Bond Lengths			
Compound **1**			
Fe(1)−Cnt1[a]	1.658(2)	C(10)−C(11)	1.432(3)
Fe(1)−Cnt2[a]	1.650(2)	C(11)−C(12)	1.186(3)
C(12)−C(13)	1.444(3)	N(14A)−C(15A)	1.356(3)
C(13)−C(15A)	1.385(3)	N(14A)−C(13A)	1.375(3)
Compound **2**			
Fe(1)−Cnt1[a]	1.653(5)	Fe(2)−Cnt3[a]	1.638(5)
Fe(1)−Cnt2[a]	1.641(4)	Fe(2)−Cnt4[a]	1.655(5)
C(10)−C(11)	1.441(11)	N(14)−C(18)	1.390(12)
C(11)−C(12)	1.159(11)	C(16)−C(17)	1.376(12)
C(12)−C(13)	1.418(12)	C(17)−C(18)	1.373(14)
C(13)−C(14)	1.379(13)	C(18)−C(19)	1.457(13)
C(13)−C(16)	1.394(14)	C(19)−C(20)	1.180(12)
C(14)−N(14)	1.345(11)	C(20)−C(21)	1.425(12)
N(14)−C(15)	1.437(13)	C(15)−P(31)	3.851
		C(15)−P(41)	4.124

Torsion Angles			
Compound **1**			
C(9)−C(10)−C(13)−C(14)	−176.2	C(9)−C(10)−C(13)−C(15A)	4.0
C(6)−C(10)−C(13)−C(14)	2.7	C(6)−C(10)−C(13)−C(15A)	−177.1
Compound **2**			
C(6)−C(10)−C(13)−C(14)	10.0	C(6)−C(10)−C(13)−C(16)	−171.4
C(9)−C(10)−C(13)−C(14)	−171.1	C(9)−C(10)−C(13)−C(16)	7.5
C(17)−C(18)−C(21)−C(22)	−11.5	N(14)−C(18)−C(21)−C(22)	165.2
C(17)−C(18)−C(21)−C(25)	174.4	N(14)−C(18)−C(21)−C(25)	−8.8

[a] Cnt = calculated centroid of cyclopentadienyl ligand.

Electronic Spectra. A striking physical difference between compounds **1** and **2** is the appearance of a low-energy absorption [λ_{max} 540 nm (ϵ_{max} 10 233) in CH_3CN] seen in the electronic spectrum of the latter that gives rise to a distinctive blue-violet coloration of solutions. Compound **1**, on the other hand, has a λ_{max} at 454 nm (ϵ_{max} 3696) for its lowest energy transition, which can be assigned to a d−d transition possessing some ligand character.[8] Although the origin of this new transition of **2** was recognized as being due to a strong metal-to-ligand charge-transfer (MLCT) transition between the ferrocene(s) and the pyridinium cation, which is a good electron acceptor,[9] the extent to which its presence might differentially perturb the electronic structure of one ferrocene over the other in this compound could only be determined by inspecting the electronic spectra for the pairs of model compounds represented by **5**/**6** and **7**/**8** of Scheme 3. Figure 3 and Table 2 present the details of a direct comparison of these data, which unequivocally establishes that a ferrocene that is directly facing the charged nitrogen atom of the pyridinium cation, as in compound **7**, has a lower energy MLCT involving this group than a ferrocene in which the charged nitrogen atom is facing away, as in compound **8**. On the basis of the delocalization scheme of structure **2b**, it can be rationalized that the lower energy MLCT transition

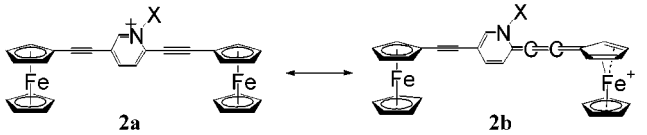

for **7** is the direct result of the pyridinium cation acceptor being in strong, direct electronic communication with the

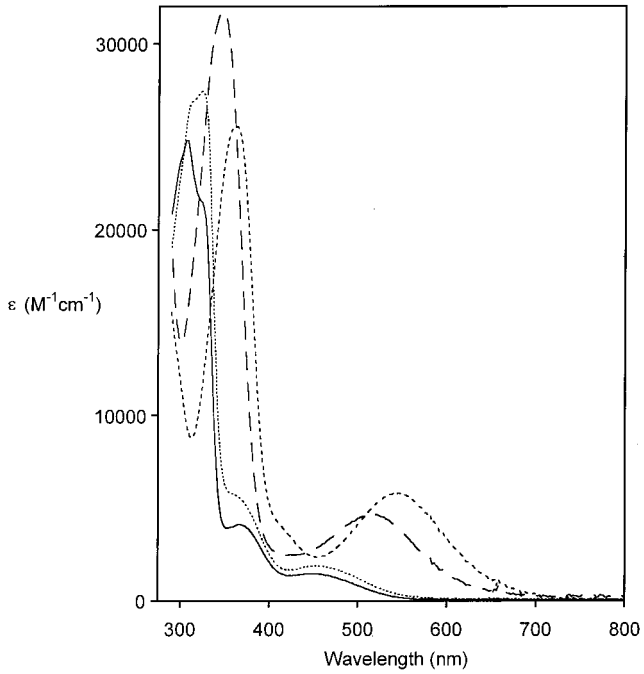

Figure 3. Electronic spectra for compounds **5** (···), **6** (—), **7** (---) and **8** (— —).

Table 2. Lowest-Energy Absorption Maxima for Compounds **1** and **2** and **5**−**8**

	λ_{max} (ϵ [M^{-1}·cm^{-1}])	
compound	CH_3CN	CH_2C1_2
1	454 (3696)	456 (5696)
2	540 (10233)	582 (18376)
5	452 (1892)	452 (1993)
6	446 (2026)	448 (1889)
7	546 (5810)	586 (9135)
8	518 (4650)	564 (9656)

ferrocene in this complex, while for **8**, it is in weaker, more indirect communication. Of further interest is the observation of a strong solvent dependency of the absorption maximum for this ferrocene−pyridinium MLCT transition that is manifested in a red-shifting to lower energy as solvent polarity decreases (see Figure 4 for compound **2**). The nature of this solvent dependency is consistent with the stabilization of an excited state that is more nonpolar than the ground state and its presence suggests that the magnitude of the ferrocene−pyridinium MLCT transition can be tuned to some degree by external factors.[9,10] As a final comment, it should be mentioned that, in contrast to **7** and **8**, the electronic spectra of the neutral pyridyl model compounds, **5** and **6**, show little difference in the position of absorption maxima as a function of which way the pyridyl nitrogen is facing the ferrocene group (see Table 2 and Figure 3). In conclusion then, the features observed in the electronic spectra of compounds **1** and **2** and **5**−**8** suggest that there is a substantial perturbation of electronic structure that occurs upon quaternization of the pyridyl nitrogen and that this should preferentially influence the redox behavior of one ferrocene over the other. Whether this perturbation is strong

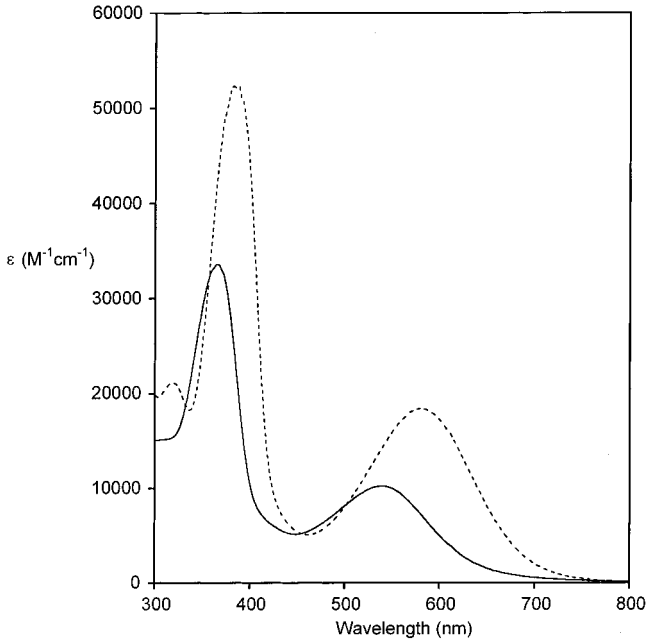

Figure 4. Solvent dependency of the lowest energy absorptions for compound **2** in CH_2Cl_2 (---) and CH_3CN (—).

Table 3. Cyclic Voltammetry (CV) and Differential Pulse Voltammetry (DPV) Analysis of Compounds **1**, **2**, and **5**−**8**[a]

	CV		DPV	
compound	$E^1_{1/2}$	$E^2_{1/2}$	$E^1_{1/2}$[b,c]	$E^2_{1/2}$[b,c]
5	0.774		0.767 (1)	
6	0.764		0.746 (1)	
7	0.890		0.871 (1)	
8	0.820		0.797 (1)	
1	0.773		0.759 (2)	
2	*d*		0.778 (1)	0.844 (1)
1[e]	0.840		0.818 (1)	
2[e]	0.955	1.12	0.929 (1)	1.09 (1)

[a] Recorded at 298 K using 1 mM of compound in a 1:1 solvent mixture of CH_2Cl_2/CH_3CN (0.1 M $[NBu_4][PF_6]$) using a glassy carbon working electrode, a Pt wire counter electrode, and a Ag/Ag^+ reference electrode. Values are reprorted relative to the redox couple for a known amount of Cp^*_2Fe added as an internal standard. [b] Calculated from $E_{pk} = E_{1/2} -$ pulse amplitude/2.[11] [c] Values in parentheses are the integrated number of electrons based on the known amount of Cp^*_2Fe added as an internal standard. [d] $E_{1/2}$ values not determined since peaks were not fully resolved by CV. [e] 0.1 M $[NBu_4][B(C_6F_5)_4]$ in CH_2Cl_2.

enough to support the proposal presented in Scheme 1, however, requires additional data.

Electrochemistry. Definitive proof that the 2,5-diethynylpyridyl bridge can serve as a viable switching element for the design depicted in Scheme 1 was provided by a comprehensive study of the electrochemical properties of **1** and **2** and **5**−**8**. Table 3 summarizes the results obtained in solution from both cyclic voltammetry (CV) and differential pulse voltammetry (DPV).[11] To begin, both electrochemical techniques revealed that all redox couples for compounds **5**−**8** are fully reversible one-electron processes at a glassy carbon electrode when a 0.1 M solution of $[n\text{-}Bu_4N][PF_6]$ in a 1:1 CH_3CN:CH_2Cl_2 solvent mixture is used as the supporting electrolyte. Interestingly, a comparison of the $E_{1/2}$ values for the two neutral isomers, **5** and **6**, showed a subtle dependence of the redox potential of the ferrocene on the relative orientation of the pyridyl nitrogen atom. Namely, when the pyridyl nitrogen is facing the ferrocene, as in **5**, the redox potential, as determined by DPV, is shifted to a slightly higher value ($\Delta E_{1/2} = 21$ mV; see Table 3). This shift is reasonable if one views a partial structure of **5** as representing a ferrocene with an electron-withdrawing conjugated imine substituent, as opposed to a partial structure of **6** in which the electronegative nitrogen atom is taken out of direct conjugated communication with the ferrocene (i.e., **5a** vs **6a**). Indeed, in comparing the $E_{1/2}$ values for the two

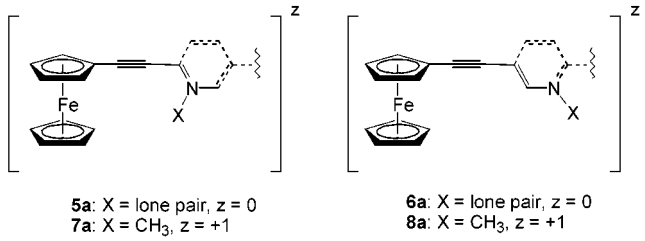

5a: X = lone pair, z = 0
7a: X = CH_3, z = +1

6a: X = lone pair, z = 0
8a: X = CH_3, z = +1

pyridinium cation isomers, **7** and **8**, it is now due to this direct conjugated communication in the former that gives rise to a greater positive shift in redox potential: cf., for **5** and **7**, $\Delta E_{1/2} = 104$ mV, and for **6** and **8**, $\Delta E_{1/2} = 51$ mV.

Having observed only a slight difference in formal potential between the two isomers, **5** and **6**, it was not too surprising to find that only a single redox couple, which integrates for two electrons by DPV using Cp^*_2Fe [$Cp^* = (\eta^5\text{-}C_5Me_5)$] as an internal standard, is observed for the model complex **1**, with an $E_{1/2}$ value approximately in the middle of those for **5** and **6**. Importantly, by CV, the observed peak separation, ΔE_p, of only 64 mV indicates that the two one-electron processes for the ferrocene groups are occurring independently of one another (cf. the theoretical limit of 59 mV).[11] Taken together then, these results firmly establish that the 2,5-diethynylpyridyl bridge is long enough to electronically isolate the two ferrocenes from each other and that its asymmetric nature does not lead to any significant perturbation in the oxidation states of the two metal centers. Hence, state 1 can be achieved.

As expected on the basis of results obtained with **7** and **8**, both CV and DPV analyses of compound **2** support the presence of two one-electron redox couples with a $\Delta E_{1/2}$ of 66 mV using the same electrolyte as before (see Table 3). While these observations support the ability to achieve state 2 with the 2,5-diethynylpyridyl bridge, we were interested in determining to what extent we could maximize the separation in redox potential between the two ferrocenes within the pyridininum cation structure. On the assumption that both nonpolar, noncoordinating solvents, and noncoordinating anions, would place the greatest amount of positive charge on the system, we turned to the CV and DPV electrochemical analysis of **1** and **2** using a 0.1 M solution of $[n\text{-}Bu_4N][B(C_6F_5)_4]$ in CH_2Cl_2.[12] As Figure 5a indicates, a single redox potential for the two ferrocenes in **1** is still observed under these conditions; however, as can be seen in Figure 5b, this change in supporting electrolyte had a dramatic effect on the $\Delta E_{1/2}$ value of **2** by pushing it to a

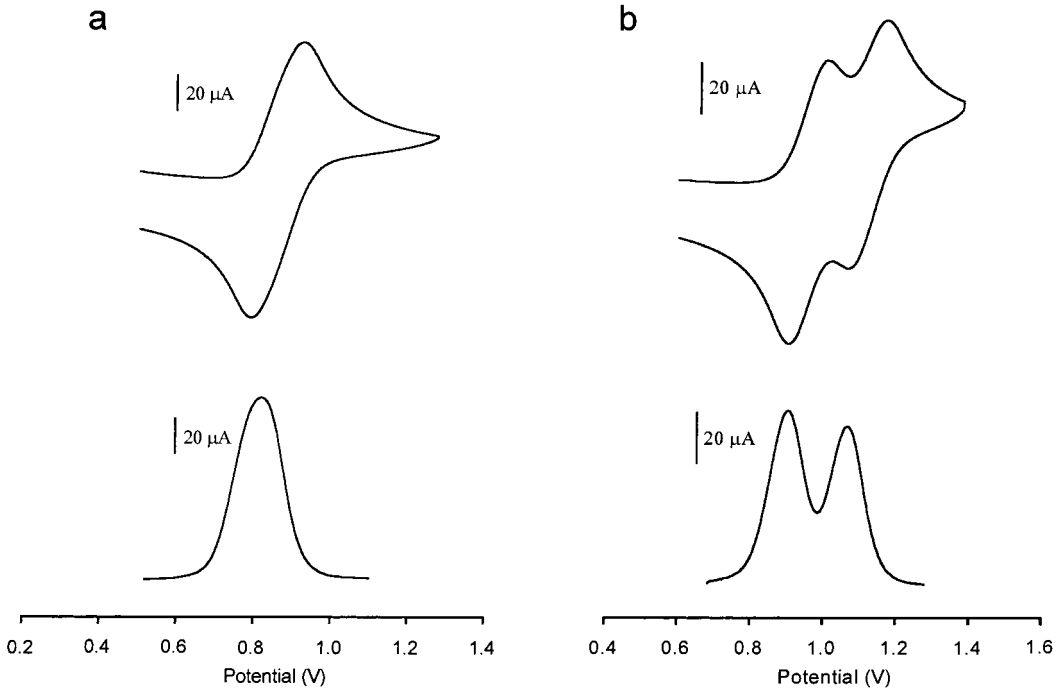

Figure 5. CV, scan rate 0.1 V s^{-1} (top) and DPV (bottom) for (a) **1** and (b) **2** in 0.1 M $[Bu_4N][B(C_6F_5)_4]$ in CH_2Cl_2 using a glassy carbon working electrode. Potentials are referenced to the redox couple of an internal decamethylferrocene standard.

value of 161 mV. These results clearly support the viability of attaining state 2 as proposed.

Having achieved the conditions for state 1 and state 2 with the 2,5-diethynylpyridyl bridge, it is important to compare our electrochemical results with those for somewhat related ferrocene-based systems that have been shown to have demonstrated switching capabilities. Briefly, Kaifer and Alvarez[13] reported that for a linked diferrocene system built using the saturated amine bridging group, $-CH_2N(R)CH_2-$, there was a small, but significant, reduction in electronic communication between the two ferrocene groups upon quaternization (or protonation) of the nitrogen atom of the bridge ($\Delta E_{1/2} = 24$ mV between the $E_{1/2}$ values for the neutral and cationic complexes). Naturally, being a symmetric bridge, formation of the cationic species affects both ferrocenes in this system equally. Regarding asymmetric bridges, Tarraga et al.[14] have just recently reported a system composed of two ferrocenes linked together by the short (relative to the 2,5-diethynylpyridyl unit) oxazole bridge. In the neutral state of this system, the two ferrocenes are once again in electronic communication, as evidenced by two redox couples being observed by CV ($\Delta E_{1/2} = 140$ mV). Surprisingly, however, upon protonation of the bridge, only a single redox couple is now observed. The authors attribute this behavior to a reduction in basicity of the oxazole nitrogen upon oxidation of the first ferrocene which then leads to deprotonation prior to oxidation of the second. While this protonation/deprotonation scheme might be viewed as forming the basis of a switching element, the mechanism by which switching is accomplished is quite different than that which is being presented here.

Conclusion. The present study serves to establish the 2,5-diethynylpyridyl linker as a potentially viable switching element for the ferrocene-based molecular diode design presented in Scheme 1. Whether this design strategy can be incorporated into working devices will naturally depend on the absolute rate of electron transfer that can be achieved within this system. To address this issue, we are presently in the process of preparing the dithiol-derivatized diferrocene molecular element depicted in Scheme 1 and intend to record its $I-V$ characteristics (for both state 1 and state 2) upon deposition across a pair of nanogap electrodes.[15] The results of these efforts will be reported in due course.

Experimental Section. All reactions were performed under a nitrogen atmosphere using standard Schlenk line techniques. All reagents were obtained from commercial suppliers and used without further purification unless otherwise indicated. Tetrahydrofuran (THF) and diethyl ether (Et_2O) were distilled from Na-benzophenone under nitrogen. Methylene chloride, diisopropylamine (DIPA), and *N*,*N*-diisopropylethylamine (Hunig's base) were distilled from calcium hydride under nitrogen. Other solvents were HPLC grade or higher. Thin-layer chromatography (TLC) analysis was performed using EM Science silica gel 60 (F254) plates (0.25 mm), and the eluted plates were observed under a UV detector. Chromatographic purifications were performed by flash chromatography on EM Science silica gel (230−400 mesh). ^1H and ^{13}C NMR spectra were taken in either chloroform-*d* or acetonitrile-d_3 at 400 and 100 MHz, respectively. High-resolution mass spectra were obtained in the FAB mode. Chemical analyses were performed by Midwest Microlab.

Preparation of 2-Bromo-5-iodopyridine. A solution of 2,5-dibromopyridine (3.00 g, 12.7 mmol) was dissolved in 100 mL of Et_2O and cooled to −78 °C. Following the dropwise addition of 9.5 mL of *n*-butyllithium (1.6 M in hexane), the

reaction mixture was stirred for 1 h at −78 °C. A quantity of iodine (4.82 g, 19 mmol) was then added and the reaction mixture was stirred for 1 h at −78 °C and then 2 h at room temperature. The reaction was monitored by TLC analysis (1:1 CH_2Cl_2/hexane) and was complete after stirring for 2 h at room temperature. The reaction mixture was extracted with 2 × 60 mL of sodium bisulfite (aq) and 2 × 60 mL sodium chloride (aq). The organic layer was separated and dried with sodium sulfate. The solvent was removed in vacuo and the crude product was purified via column chromatography using a 2:1 mixture of CH_2Cl_2 and hexane solvent system to yield 2.09 g (58%) of the desired compound as a white solid. ^{1}H NMR ($CDCl_3$): δ 7.29 (d, 1H, J = 8.3 Hz), 7.82 (dd, 1H, J = 2.4, 8.3 Hz), 8.59 (d, 1H, J = 2.4 Hz).

General Procedure for Palladium-Catalyzed Coupling Reactions. A solution of an aryl halide, terminal acetylene, $Pd(PPh_3)_2Cl_2$ (4 mol %), and CuI (4 mol %) in either diisopropylamine or a 1:1 THF/Hunig's base solvent mixture was deoxygenated using three freeze−pump−thaw cycles, and after the last cycle, the flask was backfilled with nitrogen. The reaction mixture was then stirred at 50 °C for 24−48 h. The progress of the reaction was monitored by TLC analysis. When the reaction was complete, the solvents were removed in vacuo and the residue was taken up in CH_2Cl_2 and filtered through a short silica gel column assembled in a fritted funnel. Further purification of the crude product was done via column chromatography.

*Preparation of **1***. Compound **1** was prepared using the general procedure for the palladium-catalyzed coupling reaction using 359 mg (1.71 mmol) of ethynylferrocene, 237 mg (1.00 mmol) of 2,5-dibromopyridine, and 20 mL of THF/Hunig's base (1:1). The crude product was purified by column chromatography on silica gel using a 6:1 CH_2Cl_2/hexane solvent system. The desired fractions were pooled to yield 239 mg (48%) of the title compound. Data for **1**: ^{1}H NMR ($CDCl_3$) δ 4.26 (bs, 10H), 4.29 (t, 2H, J = 2.0 Hz), 4.30 (t, 2H, J = 2.0 Hz), 4.53 (t, 2H, J = 2.0 Hz), 4.58 (t, 2H, J = 2.0 Hz), 7.41 (d, 1H, J = 8.3 Hz), 7.70 (dd, 1H, J = 2.0, 8.3 Hz), 8.66 (d, 1H, J = 2.0 Hz); ^{13}C NMR ($CDCl_3$) δ 63.8, 64.3, 69.4, 69.5, 70.2, 70.3, 71.7, 72.0, 82.8, 85.7, 91.4, 93.9, 119.5, 126.0, 138.2, 141.8, 152.2; UV (CH_3CN) λ (nm) (ϵ) 206 (60 651), 274 (18 404), 326 (30 686), 368 (11 420), 454 (3696); MS (FAB+) m/z 496 (M + 1). Anal. Calcd for $C_{29}H_{21}NFe_2$: C, 70.33; H, 4.28; N, 2.83. Found: C, 69.20; H, 4.46; N, 2.78.

*Preparation of **2***. Compound **2** was prepared using 42 mg (85 μmol) of **1**, 73 mg (0.51 mmol) of iodomethane in 2 mL of CH_2Cl_2, and 3 mL of CH_3CN. The reaction mixture was heated to 55 °C and stirred for 18 h. When the reaction was complete by TLC analysis (5:1 CH_2Cl_2/hexane), it was filtered through a short silica gel column assembled in a fritted funnel using 100 mL of acetone. The solvents were then removed in vacuo, and the dark purple residue was dissolved in a minimum amount of CH_3CN and 0.5 g of ammonium hexafluorophosphate was added. Distilled water was added to the solution to precipitate the desired product, and the solid was then isolated via suction filtration, washed with ample amounts of distilled water, and dried in a vacuum oven overnight to yield 41.3 mg (74%) of the title compound as a dark purple solid. Data for **2**: ^{1}H NMR ($CDCl_3$) δ 4.30 (s, 5H), 4.35 (s, 5H), 4.38 (t, 2H, J = 2.0 Hz), 4.42 (s, 3H), 4.57 (t, 2H, J = 2.0 Hz), 4.63 (t, 2H, J = 2.0 Hz), 4.72 (t, 2H, J = 2.0 Hz), 7.82 (d, 1H, J = 8.3 Hz), 8.15 (bd, 1H, J = 8.3 Hz), 8.72 (bs, 1H); ^{13}C NMR (CD_3CN) δ 48.3, 60.4, 62.9, 71.3, 71.4, 71.8, 72.9, 73.0, 74.0, 78.9, 79.9, 100.4, 113.7, 123.0, 131.4, 137.4, 145.7, 148.6; UV (acetonitrile) λ (nm) (ϵ) 214 (40 748), 276 (19 661), 366 (33 628), 540 (10 233); MS (FAB+) m/z 510 (M^+). Anal. Calcd for $C_{30}H_{24}NFe_2PF_6$: C, 54.99; H, 3.70; N, 2.14. Found: C, 54.69; H, 3.74; N, 2.19.

*Preparation of **3***. Compound **3** was prepared using the general procedure for the palladium-catalyzed coupling reaction using 46 mg (2.20 mmol) of ethynylferrocene, 306 mg (1.29 mmol) of 2,5-dibromopyridine, and 24 mL of THF/Hunig's base (1:1). The crude product was purified by column chromatography on silica gel using a 3:1 CH_2Cl_2/hexane solvent system. The desired fractions were pooled to yield 408 mg (87%) of the desired compound. Data for **3**: ^{1}H NMR ($CDCl_3$) δ 4.26 (s, 5H), 4.29 (t, 2H, J = 2.0 Hz), 4.57 (t, 2H, J = 2.0 Hz), 7.35 (d, 1H, J = 8.3 Hz), 7.77 (dd, 1H, J = 2.0, 8.3 Hz), 8.64 (d, 1H, J = 2.0 Hz); ^{13}C NMR ($CDCl_3$) δ 63.5, 69.6, 70.2, 72.0, 84.7, 91.1, 119.2, 127.7, 138.9, 142.4, 151.2; UV (chloroform) λ (nm) (ϵ) 256 (17 556), 302 (17 955), 360 (3681), 452 (1153); MS (FAB+) m/z 365/367 (M^+); Anal. Calcd for $C_{17}H_{12}NBrFe$: C, 55.78; H, 3.31; N, 3.83. Found: C, 56.08; H, 3.43; N, 3.83.

*Preparation of **4***. Compound **4** was prepared using the general procedure for the palladium-catalyzed coupling reaction using 321 mg (1.53 mmol) of ethynylferrocene, 651 mg (2.29 mmol) of 2-bromo-5-iodopyridine, and 20 mL of diisopropylamine. The crude product was purified by column chromatography on silica gel using a 3:1 CH_2Cl_2/hexane solvent system. The desired fractions were pooled to yield 456 mg (81%) of the title compound. Data for **4**: ^{1}H NMR ($CDCl_3$) δ 4.24 (s, 5H), 4.29 (t, 2H, J = 2.0 Hz), 4.52 (t, 2H, J = 2.0 Hz), 7.44 (d, 1H, J = 8.3 Hz), 7.60 (dd, 1H, J = 2.0, 8.3 Hz), 8.45 (d, 1H, J = 2.0 Hz); ^{13}C NMR ($CDCl_3$) δ 63.9, 69.4, 70.2, 71.7, 81.3, 93.9, 120.6, 127.7, 140.2, 140.4, 152.2; UV (chloroform) λ (nm) (ϵ) 258 (19 244), 298 (17 585), 354 (3061), 448 (937); MS (FAB+) m/z 365/367 (M^+). Anal. Calcd for $C_{17}H_{12}NBrFe$: C, 55.78; H, 3.31; N, 3.83. Found: C, 55.48; H, 3.22; N, 3.60.

*Preparation of **5***. Compound **5** was prepared using the general procedure for the palladium-catalyzed coupling reaction using 528 mg (1.44 mmol) of **3**, 849 mg (8.64 mmol) of trimethylsilylacetylene, and 25 mL of THF/Hunig's base (1:1). The crude product was purified by column chromatography on silica gel using a 4:1 CH_2Cl_2/hexane solvent system. The desired fractions were pooled to yield 518.3 mg (94%) of the title compound. Data for **5**: ^{1}H NMR ($CDCl_3$) δ 0.28 (s, 9H), 4.26 (s, 5H), 4.29 (t, 2H, J = 2.0 Hz), 4.57 (t, 2H, J = 2.0 Hz), 7.39 (d, 1H, J = 8.3 Hz), 7.69 (dd, 1H, J = 2.0, 8.3 Hz), 8.64 (d, 1H, J = 2.0 Hz); ^{13}C NMR ($CDCl_3$) δ −0.1, 63.6, 69.6, 70.3, 72.1, 85.5, 91.9, 99.8, 101.7, 118.5, 125.9, 138.9, 142.8, 152.9; UV (acetonitrile) λ (nm) (ϵ) 204 (42 010), 272 (21 585), 324 (27 477), 356 (5847), 452 (1892);

MS (FAB+) *m/z* 384 (M + 1). Anal. Calcd for $C_{22}H_{21}NFeSi$: C, 68.92; H, 5.53; N, 3.65. Found: C, 68.93; H, 5.66; N, 3.56.

*Preparation of **6**.* Compound **6** was prepared using the general procedure for the palladium-catalyzed coupling reaction using 108 mg (0.30 mmol) of **4**, 175 mg (1.78 mmol) of trimethylsilylacetylene, and 8 mL of THF/Hunig's base (1:1). The crude product was purified by column chromatography on silica gel using a 4:1 CH_2Cl_2/hexane solvent system. The desired fractions were pooled to yield 108 mg (94%) of the title compound. Data for **6**: ^{1}H NMR ($CDCl_3$) δ 0.28 (s, 9H), 4.26 (s, 5H), 4.29 (t, 2H, $J = 2.0$ Hz), 4.52 (t, 2H, $J = 2.0$ Hz), 7.40 (d, 1H, $J = 8.3$ Hz), 7.69 (dd, 1H, $J = 2.0, 8.3$ Hz), 8.64 (d, 1H, $J = 2.0$ Hz); ^{13}C NMR ($CDCl_3$) δ −0.2, 64.1, 69.4, 70.2, 71.7, 82.6, 94.4, 96.7, 103.7, 120.6, 126.7, 138.1, 140.9, 152.2; UV (acetonitrile) λ (nm) (ϵ) 208 (45 906), 274 (2831), 306 (34 056), 366 (5577), 446 (2026); MS (FAB+) *m/z* 384 (M + 1). Anal. Calcd for $C_{22}H_{21}NFeSi$: C, 68.92; H, 5.53; N, 3.65. Found: C, 68.63; H, 5.63; N, 3.55.

*Preparation of **7**.* Compound **7** was prepared using 94 mg (0.25 mmol) of **5**, 211.4 mg (1.47 mmol) of iodomethane in 2 mL of CH_2Cl_2, and 3 mL of CH_3CN. The reaction mixture was heated to 70 °C and stirred for 18 h. The reaction was determined to be complete by TLC analysis using a 5:1 CH_2Cl_2/hexane solvent system. The solvent was then removed and the dark maroon residue was dissolved in a minimum amount of CH_3CN, and 0.5 g of ammonium hexafluorophosphate was added. Distilled water was added to the solution to precipitate the desired product, and the solid was then isolated via suction filtration, washed with ample amounts of distilled water, and dried in a vacuum oven overnight to yield 116 mg (87%) of the title compound as a dark purple solid. Data for **7**: ^{1}H NMR (CD_3CN) δ 0.29 (s, 9H), 4.25 (s, 3H), 4.35 (s, 5H), 4.62 (t, 2H, $J = 2.0$ Hz), 4.81 (t, 2H, $J = 2.0$ Hz), 7.95 (d, 1H, $J = 8.3$ Hz), 8.28 (dd, 1H, $J = 2.0, 8.3$ Hz), 8.66 (bs, 1H); ^{13}C NMR ($CDCl_3$) δ −0.5, 48.1, 59.0, 71.3, 72.3, 73.3, 78.5, 96.5, 107.6, 116.2, 121.8, 130.3, 137.4, 145.2, 148.1; UV (acetonitrile) λ (nm) (ϵ) 204 (39 511), 280 (19 327), 362 (25 536), 546 (5810); MS (FAB+) *m/z* 398 (M^+). Anal. Calcd for $C_{23}H_{24}NFeSiPF_6$: C, 50.83; H, 4.46; N, 2.58. Found: C, 49.65; H, 4.42; N, 2.75.

*Preparation of **8**.* Compound **8** was prepared using 92 mg (0.24 mmol) of **6**, 206.0 mg (1.45 mmol) of iodomethane in 2 mL of CH_2Cl_2, and 3 mL of CH_3CN. The reaction mixture was heated to 70 °C and stirred for 18 h. The reaction was determined to be complete by TLC analysis using a 5:1 CH_2Cl_2/hexane solvent system. The solvent was then removed, and the dark maroon residue was dissolved in a minimum amount of CH_3CN and 0.5 g of ammonium hexafluorophosphate was added. Distilled water was added to the solution to precipitate the desired product, and the solid was then isolated via suction filtration, washed with ample amounts of distilled water, and dried in a vacuum oven overnight to yield 109 mg (84%) of the title compound as a dark maroon solid. Data for **7**: ^{1}H NMR (CD_3CN) δ 0.35 (s, 9H), 4.28 (s, 3H), 4.30 (s, 5H), 4.45 (t, 2H, $J = 2.0$ Hz), 4.63 (t, 2H, $J = 2.0$ Hz), 7.98 (d, 1H, $J = 8.3$ Hz), 8.35 (dd, 1H, $J = 2.0, 8.3$ Hz), 8.74 (bs, 1H); ^{13}C NMR ($CDCl_3$) δ −0.8, 47.9, 61.6, 70.6, 70.7, 72.5, 79.5, 93.4, 103.4, 119.0, 125.4, 131.5, 133.9, 144.7, 148.3; UV (acetonitrile) λ (nm) (ϵ) 202 (52 588), 276 (29 013), 348 (31 704), 518 (4650); MS (FAB+) *m/z* 398 (M^+). Anal. Calcd for $C_{23}H_{24}NFeSiPF_6$: C, 50.83; H, 4.46; N, 2.58. Found: C, 50.64; H, 4.37; N, 2.51.

Table 4. Crystal Structure and Refinement Data for Compounds **1** and **2**

	1	**2**
formula	$C_{29}H_{21}NFe_2$	$C_{30}H_{24}NFe_2PF_6$
M_w	495.17	655.17
space group	monoclinic $P2(1)/n$	monoclinic $P2(1)/c$
a (Å)	6.0695(7)	12.118(9)
b (Å)	21.876(3)	7.669(6)
c (Å)	7.9107(9)	28.787(16)
β (deg)	93.407(2)	96.241(15)
V (Å^3)	1048.5(2)	2660(3)
Z	2	4
D_{calcd} (Mg/m^3)	1.568	1.636
abs coeff (mm^{-1})	1.401	1.215
$F(000)$	508	1328
crystal size, mm^3	0.500 × 0.150 × 0.066	0.520 × 0.067 × 0.020
θ range (deg)	1.86−27.58	1.69−25.00
index ranges	$-7 \le h \le 7$ $-28 \le k \le 28$ $-10 \le l \le 10$	$-14 \le h \le 14$ $-9 \le k \le 9$ $-34 \le l \le 34$
no. of reflns collected	16 262	32 162
no. of ind reflns	2430 ($R_{int} = 0.0486$)	4671 ($R_{int} = 0.0850$)
abs corr	integration	empirical, SADABS
refinement method	full-matrix least-squares on F^2	
data/restraints/params	2430/6/195	4671/45/402
goodness of fit on F^2	0.956	1.118
final R indices [$I > 2\sigma(I)$]	$R1 = 0.0349$ $wR2 = 0.0864$	$R1 = 0.0784$ $wR2 = 0.1881$
largest diff peak and hole (e Å^{-3})	0.618 and −0.268	0.603 and −0.738

Electrochemical Procedures. Methylene chloride (HPLC grade) and acetonitrile (HPLC grade) were distilled from calcium hydride under nitrogen. Tetrabutylammonium hexafluorophosphate was recrystallized three times from ethanol and dried in a vacuum oven at 80 °C for several days. The tetrabutylammonium tetrakis(pentafluorophenyl)borate salt was prepared according to the published procedure.[12] A standard three-electrode cell was utilized at ambient temperatures under an atmosphere of argon. A glassy carbon disk was used as the working electrode and the counter electrode was a Pt wire. The reference electrode was a silver wire, but all potentials are recorded relative to the decamethylferrocene/decamethylferrocenium couple through the addition of this internal standard at the end of each electrochemical analysis. All CV traces were taken at a scan rate of 0.1 V s^{-1}. Differential pulse voltammetry experiments utilized a pulse amplitude of 50 mV and a step potential of 2 mV.

Crystallography. As a general procedure, for **1**, a reddish-orange crystalline plate with dimensions 0.50 × 0.066 × 0.075 mm^3 was placed and optically centered on the Bruker SMART CCD system at −80 °C. The initial unit cell was indexed using a least-squares analysis of a random set of reflections collected from three series of 0.3° wide ω scans

(25 frames/series) that were well distributed in reciprocal space. Data frames were collected [Mo Kα] with 0.3° wide ω-scans, 20 s/frame, 606 frames per series, 6 complete series including an additional full run of the first series for decay purposes, a crystal to detector distance of 4.94 cm, providing a complete sphere of data to $2\theta_{max} = 55.1°$. A total of 16 262 reflections were collected and corrected for Lorentz and polarization effects and absorption; first through face indexing in XPREP then Blessing's method as incorporated into the program SADABS with 2430 unique reflections [R(int) = 0.0486]. Data for compound **2** were collected in a similar fashion, with the variables listed in Table 4.

All crystallographic calculations were performed on a personal computer (PC) with dual Pentium 450 MHz processors and 256 MB of extended memory. For both structures the SHELXTL program package XPREP was implemented to determine the probable space group and set up the initial files. System symmetry and systematic absences indicated the centrosymmetric space group $P2_1/c$ (no. 14). The structures were determined by direct methods with the successful location of nearly all non-hydrogen atoms using the program XS. The structures were refined with XL and after the initial refinement difference Fourier cycle, additional non-hydrogen atoms were located and input for both structures. After one of these refinement difference Fourier cycles, all of the non-hydrogen atoms were refined isotropically, then anisotropically. Because of the nature of **1** and the inversion center at its center, the unique nitrogen atom comprising the central ring was compelled to be in two locations, each 50% of the time. The PF_6 group in **2** was found to occupy two overlapping positions and their occupancies were modeled. For **1**, the hydrogen atoms were located directly from difference Fourier maps and allowed to refine freely ($x0yzU$), while in the case for **2**, the hydrogen atoms were placed in calculated positions. The final difference Fourier maps were featureless, indicating that the structures for **1** and **2** were both correct and complete.

Acknowledgment. This work was supported through the NSF MRSEC program (DMR-00−80008) for which we are grateful.

Supporting Information Available: ^{1}H NMR spectra for compounds **1**−**4** and additional details of the crystal structural analyses of **1** and **2**, including tables for the complete listing of atom positions, isotropic and anisotropic temperature factors, bond distances and bond angles. This material is available free of charge via the Internett at http://pubs.acs.org.

References

(1) (a) Ratner, M.; Jortner, J. *Molecular Electronics*; Blackwell Science: Malden, MA, 1997. (b) Tour, J. M. *Acc. Chem. Res*. **2000**, *33*, 791−804. (c) Collier, C. P.; Wong, E. W.; Belohradsky, M.; Raymo, F. M.; Stoddart, J. F.; Kuekes, P. J.; Williams, R. S.; Heath, J. R. *Science* **1999**, *285*, 391−394.

(2) Togni, A., Hayashi, T., Eds. *Ferrocenes*; VCH Publishers: New York, 1995.

(3) (a) Flanagan, J. B.; Margel, S.; Bard, A. J.; Anson, F. C. *J. Am. Chem. Soc*. **1978**, *100*, 4248−4253. (b) Daum, P.; Murray, R. W. *J. Phys. Chem*. **1981**, *85*, 389−396. (c) Rosenblum, M.; Nugent, H. M.; Jang, K. S.; Labes, M. M.; Cahalane, W.; Klemarczyk, P.; Reiff, W. M. *Macromolecules* **1995**, *28*, 6330−6342. (d) Watanabe, M.; Nagasaka, H.; Ogata, N. *J. Phys. Chem*. **1995**, *99*, 12294−12300. (e) Lee, W. Y.; Hostetler, M. J.; Murray, R. W.; Majda, M. *Isr. J. Chem*. **1997**, *37*, 213−223.

(4) For previous studies and a discussion of electron-hopping conduction within solid-state materials, see: Terrill, R. H.; Murray, R. W. In *Molecular Electronics*; Blackwell Science: Malden, MA, 1997; Chapter 6 and references therein.

(5) Rosenblum, M.; Brawn, N.; Papenmeier, J.; Applebaum, M. *J. Organomet. Chem*. **1966**, *6*, 173−180.

(6) Tilley, J. W.; Zawoiski, S. *J. Org. Chem*. **1988**, *53*, 386-390.

(7) Details provided in the Supporting Information.

(8) (a) Sohn, Y. S.; Hendrickson, D. N.; Gray, H. B. *J. Am. Chem. Soc*. **1971**, *93*, 3606−3612. (b) Calabrese, J. C.; Cheng, L. T.; Green, J. C.; Marder, S. R.; Tam, W. *J. Am. Chem. Soc*. **1991**, *113*, 7227−7232.

(9) (a) Marder, S. R.; Perry, J. W.; Tiemann, B. G.; Schaefer, W. P. *Organometallics* **1991**, *10*, 1896−1901. (b) Lin, J. T.; Wu, J. J.; Li, C. S.; Wen, Y. S.; Lin, K. J. *Organometallics* **1996**, *15*, 5028−5034. (c) Mata, J. A.; Uriel, S.; Llusar, R.; Peris, E. *Organometallics* **2000**, *19*, 3797−3802. (d) Dieguez, M.; Collomb, M. N.; Crabtree, R. H. *J. Organomet. Chem*. **2000**, *608*, 146−152.

(10) Turro, N. J. *Modern Molecular Photochemistry*; Benjamin/Cummings Publishing Co., Inc.: Menlo Park, CA, 1978.

(11) Wang, J. *Analytical Electrochemistry*; Wiley-VCH: New York, 2000.

(12) LeSuer, R. J.; Geiger, W. E. *Angew. Chem., Int. Ed. Engl*. **2000**, *39*, 248−250.

(13) Alvarez, J.; Kaifer, A. E. *Organometallics* **1999**, *18*, 5733−5734.

(14) Tarraga, A.; Molina, P.; Curiel, D.; Velasco, M. D. *Organometallics* **2001**, *20*, 2145−2152.

(15) (a) Morpurgo, A. F.; Marcus, C. M.; Robinson, D. B. *Appl. Phys. Lett*. **1999**, *74*, 2084−2086. (b) Bezryadin, A.; Dekker: C.; Schmid, G. (b) Porath, D.; Bezryadin, A.; de Vries, S.; Dekker: C. *Nature* **2000**, *403*, 635−638.

NL010038P